Chapter 3

Adding Large Scale Structure data into the search

Foreword

This chapter is based on the e-print (submitted to *Physical Review D*)

> **Searching for primordial localized features with CMB and LSS spectra**
>
> Bin Hu, Jesús Torrado
>
> Submitted to Physical Review D
>
> Preprint in arXiv:1410.4804 [astro-ph.CO]

The results presented in it and reproduced here are the product of the combined effort of all its authors, who, as is customary in Theoretical Cosmology, appear in alphabetical order. In this short chapter, I reproduce a major part of the original publication, omitting the introductory content which has already been presented in the previous chapters.

Abstract

Inspired by the study of mild transient reductions in the speed of sound of the adiabatic mode during inflation, we search for a primordial localized feature imprinted in cosmic microwave background and large-scale structure formation observables. We find some common oscillatory patterns both in the Planck CMB temperature power spectrum and the WiggleZ galaxy spectrum. By performing independent searches with these two data sets, we find a coincidence in the most significant mode previously found by Achúcarro *et al.* 2013 by using only Planck data. Furthermore, the joint data analysis shows that the oscillation frequency of

the feature gets better constrained, and the amplitude marginally deviates from zero, unlike what was observed using only Planck data. Besides the parameter estimation, we also discuss the Bayesian evidence. The addition of WiggleZ data mildly enhances the significance of the best mode found in the Planck data.

3.1 Introduction

As discussed in the last chapter there exist several hints of oscillatory signals in the CMB power spectrum [10, 7] and bispectrum [8]. This motivates a search for such kind of features produced by inflationary scenarios beyond canonical single-field.[1] A short review of the literature on those attempts can be seen in the Introduction of the last chapter. In none of those cases the statistical significance of the extended models has been found to be high enough to claim a detection, with the improvement of experimental accuracy we are now at the threshold of verifying or falsifying these models.

In this thesis we focus on searching for oscillatory features in the scenario of a transient reduction in the speed of sound, reviewed in section 1.3.4. Our test case, introduced in the last chapter (and in [2]), consists of a gaussian reduction in the speed of sound occurring within the window of e-folds corresponding to the angular scales probed by CMB and large-scale structure (LSS) surveys. Its functional form is consistent with a reduction in the speed of sound resulting from a soft turn along the inflationary trajectory in a multi-field theory in which the mass hierarchy is large enough to allow for an effective single-field description [4, 3, 12, 5] (though one should keep in mind that a similar reduction in the speed of sound may result from a different high-energy completion of the effective field theory).

Since it is the same curvature perturbations that set the initial conditions for CMB anisotropies and large-scale structure distributions, the primordial oscillatory signals should be imprinted in all the observables of CMB anisotropy and LSS tracers, like CMB spectra, bispectra, galaxy spectra, etc. Based on this consideration, in this chapter and in the original publication [17] we search for primordial oscillatory features from a transient reduction in the speed of sound of adiabatic curvature perturbations via both CMB anisotropy temperature spectrum of the Planck satellite as well as galaxy distribution spectrum of the WiggleZ telescope. The rest of this chapter is organised as follows. In sec. 3.2, we will briefly review the theoretical set-up. In sec. 3.3, we will introduce the methodology of parameter estimation and model selection which is adopted in this work as well as the data sets used. Then, we arrive at our results and discuss them in sec. 3.4. Finally, we conclude in sec. 3.5.

[1] By canonical single-field we mean slow-roll regime, Bunch-Davies vacuum, canonical kinetic terms and minimal coupling to gravity, with speed of sound $c_s = 1$.

3.2 Review of the model

In this chapter and the original publication [17], we search for localised features due to a transient reduction in the speed of sound of the adiabatic mode during inflation (see sec. 1.3.4) parametrised as a gaussian in e-folds. The shape tested here is the same previously tested against Planck CMB data only, and it is described in detail in section 2.2 in the last chapter, together with the allowed ranges of its parameters. Very briefly, the resulting feature in the primordial spectrum is

$$\frac{\Delta\mathcal{P}}{\mathcal{P}}(k) = k\int_{-\infty}^{0} d\tau\ u(\tau)\sin(2k\tau)\ , \tag{3.1}$$

where the reduction in the speed of sound is parametrised as

$$u = 1 - c_s^{-2} = B\, e^{-\beta(N-N_0)^2} = B\, e^{-\beta\left(\ln\frac{\tau}{\tau_0}\right)^2}\ . \tag{3.2}$$

The parameters of the feature: the amplitude $B < 0$, the sharpness $\beta > 0$, and the instant of maximal reduction N_0 (or $\tau_0 < 0$) fall within the region

$$\mathcal{O}(\epsilon,\eta) \ll |B| \ll 1\ , \tag{3.3a}$$

$$\frac{50}{N_{\rm CMB}^2} < \beta \ll \frac{2e}{B^2}\ , \tag{3.3b}$$

$$4.3 \leq \ln(-\tau_0) \leq 6.0\ . \tag{3.3c}$$

For the precise meaning of the quantities that appear here, see sec. 2.2.

3.3 Methodology and data sets

In this work we solve the Einstein-Boltzmann hierarchy by using CAMB [20] and sample the parameter space using different approaches in order to fulfil two different purposes. On one hand, for parameter estimation, we use the thermodynamic Markov chain Monte Carlo (MCMC) sampler, CosmoMC [19]. In detail, we use a Metropolis-Hastings algorithm to generate chains of samples for a set of cosmological parameters. On the other hand, for Bayesian evidence computation and model selection, we adopt the multi-modal nested sampler, MultiNest [15, 16, 14] which implements an extended form of the nested sampling algorithm [28, 27, 22, 21, 26]. This is because the dependence of the evidence on the prior requires that the prior space is adequately sampled, even in the regions of low likelihood. This makes evidence evaluation at least an order of magnitude more costly than parameter estimation.

In what follows we make a brief review of the concepts of evidence and Bayesian ratio. The Bayesian ratio is defined as the ratio of the probabilities of each of the

two models being the true one underlying a given a set of data **D**:

$$R = \frac{P(M_1|\mathbf{D})}{P(M_0|\mathbf{D})} = \frac{\mathcal{Z}_1}{\mathcal{Z}_0}\frac{P(M_1)}{P(M_0)} = \frac{\mathcal{Z}_1}{\mathcal{Z}_0} \,. \tag{3.4}$$

Here, $P(M_1)/P(M_0)$ is the probability ratio for the two models *a priori*, which is conventionally set to unity; the *evidence* $\mathcal{Z}$ of a model M is the marginalised likelihood of the data, i.e. the probability of having obtained the data **D** integrated over all possible values of the model parameters $\boldsymbol{\theta}$:

$$\mathcal{Z} = \int \mathcal{L}(\mathbf{D}|M(\boldsymbol{\theta}))\,\pi(\boldsymbol{\theta})\,\mathrm{d}^D\boldsymbol{\theta} \,, \tag{3.5}$$

where $\mathcal{L}(\mathbf{D}|M(\boldsymbol{\theta}))$, $\pi(\boldsymbol{\theta})$ and D are, respectively, the likelihood of the data, the prior of the parameters in the model and the dimensionality of the parameter space. In this work, we will use M_1 and M_0 to denote the feature and featureless ΛCDM models; the cosmological parameter ranges we studied are listed in table 3.1. And the multidimensional integration in eq. (3.5) was sampled via the multi-modal implementation of the nested sampling algorithm MultiNest [15, 16, 14].

Parameter	Range (min, max)
$\Omega_b h^2$	$(0.005, 0.100)$
$\Omega_c h^2$	$(0.01, 0.99)$
$100\vartheta_*$	$(0.5, 10.0)$
τ_{reio}	$(0.01, 0.80)$
n_s	$(0.9, 1.1)$
$\ln(10^{10}A_s^2)$	$(2.7, 4.0)$
B	$(-0.2, 0)$
$\ln\beta$	$(0, 7.5)$
$\ln(-\tau_0)$	$(4.3, 6.0)$

Table 3.1: List of the parameters used in the multi-modal nested sampling. Besides these parameters, we also sample and marginalise over the fourteen nuisance parameters of the Planck likelihood and one bias parameter of the WiggleZ likelihood. We have sampled B up to -0.5, but nothing interesting was found beyond the upper value cited in this table.

The Bayesian evidence measures the predictivity of a model: the integral in eq. (3.5) is bigger the more amount of likelihood mass falls inside the regions with substantial prior probability, and also the smaller is the volume $\mathcal{V}$ of the parameter space allowed by the theory, since the prior distribution goes roughly like $\pi \sim \mathcal{V}^{-1}$. In turn, the Bayesian ratio quantifies the relative predictivity of two models given a data set: if its value is much smaller than one, the model M_0 is a more likely explanation of the data than the model M_1, and vice versa. In the

frequentist approach, this is comparable to the increase of p-values[2] due to the *look-elsewhere effect*. For example, in particle physics, if one allows the predicted mass of a particle to vary within a broad range, the p-value of an apparent peak in particle production with a corresponding mass within this range will increase, just because a wider range of energies makes a random, non-physical peak-like feature more likely. Correspondingly, this indicates that the evidence of this model with a new parameter, like the new particle's mass, gets reduced.

On the other hand, the Bayesian ratio can also be used as an indicator of the correlation between two data sets with respect to an extended model M_1 based on a simpler model M_0: if the predictivity of the extended model with respect to the basis model increases when adding the new data set, this is an indication of the regions of high probability in the likelihood of the extended model being similar in the two data sets. Otherwise, the product of the likelihoods of both data sets would amount to a smaller evidence ratio than that of the single data sets.

As for the data sets, we use the measurements of CMB temperature anisotropy[3] [9] from the first data release of the Planck survey. Its temperature power-spectrum likelihood is divided into low-ℓ ($\ell < 50$) and high-ℓ ($\ell \geq 50$) parts (see sec. 1.5.4). In order to break the well-known parameter degeneracy between the reionisation optical depth τ_{reio} and the scalar index n_s, the low-ℓ WMAP polarisation likelihood (WP) is used [9]. Finally, the unresolved foregrounds are marginalised over, assuming wide priors on the relevant nuisance parameters as described in [6].

Since several interesting feature modes are hinted at by using only Planck temperature spectrum (see chapter 2 or [2]), a natural step is to cross check these results with other observables seeded by the same initial conditions, coming from different experiments whose systematic uncertainties are different from Planck's. We use the measurements of the galaxy power spectrum made by the WiggleZ Dark Energy Survey.[4] As described in [24], we use the power spectrum measured from spectroscopic redshifts of 170 352 blue emission line galaxies over a volume of $\sim 1\,\mathrm{Gpc}^3$ [13]. The covariance matrices as given in [24] are computed using the method described by [11]. The best model proposed for non-linear corrections to the matter power spectrum was calibrated against simulations. It has already been demonstrated that linear theory predictions are as good a fit to the data as the calibrated model up to $k \sim 0.2\,h/\mathrm{Mpc}$ [24, 25]. For these reasons we restrict ourselves to scales smaller than $k_{\mathrm{max}} = 0.2\,h/\mathrm{Mpc}$ and use the linear theory prediction only. We also marginalise over a linear galaxy bias for each of the four

[2]From Wikipedia.org, a p-value is the probability of obtaining a test statistic result at least as extreme as the one that was actually observed, assuming that the null hypothesis is true. A researcher will often "reject the null hypothesis" when the p-value turns out to be less than a predetermined significance level, often 0.05 or 0.01. Such a result indicates that the observed result would be highly unlikely under the null hypothesis.

[3]`http://pla.esac.esa.int/pla/aio/planckProducts.html`

[4]`http://smp.uq.edu.au/wigglez-data`

redshift bins.

3.4 Results and discussion

In order to justify or falsify this model, we should go beyond CMB observables from the Planck satellite. A feature in the primordial spectrum of density perturbations will seed both CMB anisotropies and the tracers of matter perturbation, such as the galaxy distribution. Thus, if those features are big enough we should observe them via all those windows.

Based on the findings of the previous study with Planck temperature power spectrum (see chapter 2 and [2, 1]), we sample the same region of the parameter space using *only* the galaxy power spectrum from the WiggleZ Dark Energy Survey. The result is shown in fig. 3.1(a). In particular we show the profile likelihood of the sample in the plane $(\ln\beta, -\ln(-\tau_0))$. The upper limit of $\ln(-\tau_0)$ has been slightly extended, and the lower one slightly shrunk, in order to limit the interval to the region in which the improvement in the likelihood is significant (but we will later restore the limits of chapter 2 in the evidence computation).

As we can see, in the WiggleZ posterior there exist three diffused modes. In particular, comparing figs. 3.1(a) and 3.1(b) with the naked eye there seems to exist a coincidence between WiggleZ and Planck results around $\ln(-\tau_0) \sim 6.0$, $\ln(-\tau_0) \sim 5.55$ and $\ln(-\tau_0) \sim 5.3$, which were three of the most significant modes detected in the previous work [2], named respectively modes $\mathcal{A}$, $\mathcal{B}$ and $\mathcal{C}$ (see table 2.1). In order to test such coincidence, we repeated the search combining both data sets. The results are reported in fig. 3.1(c). The well-isolated modes previously found in the Planck data are accurately reproduced (compare figs. 3.1(b) and 3.1(c), and also see fig. 3.2(a)). In addition we observe an unfolding of mode $\mathcal{A}$ and a new mode at $\ln(-\tau_0) \sim 6.3$ which survives the addition of the WiggleZ data; both of them will be the subject of future work. We have checked that there exists an enhancement of more than 20% in the value of the likelihood improvement ($\Delta \ln \mathcal{L}$) in modes $\mathcal{B}$ and $\mathcal{C}$, while that of mode $\mathcal{A}$ shows no enhancement.

Later, we isolated and re-sampled using MCMC methods each of the four individual modes found in [2] (see fig. 3.2) with the joint data sets. The corresponding results are shown in the fig. 3.2(a). We can see that the individual modes are separated quite well in the $\ln(-\tau_0)$ direction.

If we force ourselves to focus on one particular mode, such as mode $\mathcal{B}$, we can obtain quite stringent constraints on the feature parameters, like those demonstrated in chapter 2, e.g. in table 2.1 or fig. 2.6. However, finding stringent constraints does not mean that this result has a very strong statistical significance, because the parameter space volume of the feature model is much larger than that of the *vanilla* ΛCDM model. So, even if there exists a local patch in the parameter space with highly peaked likelihood, the evidence of this signature could still be suppressed greatly by the big volume of the extra parameter space,

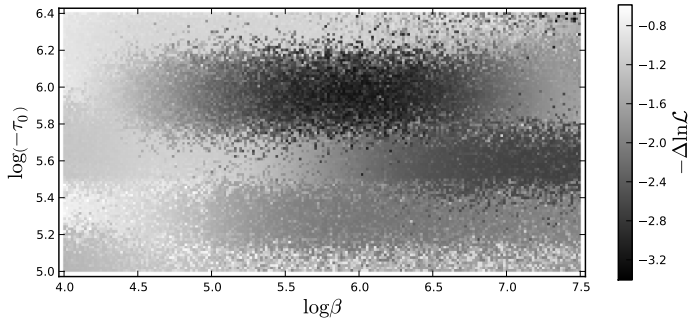

(a) WiggleZ

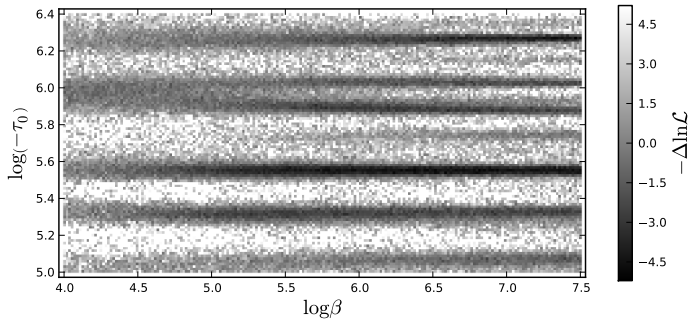

(b) Planck

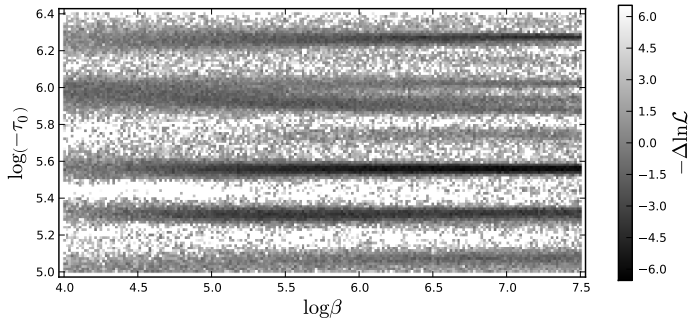

(c) Planck+WiggleZ

Figure 3.1: Profile parameter distribution of the MCMC sampling in the $(\ln\beta, -\ln(-\tau_0))$ plane, for the different combinations of data sets. It shows the coincidence between the fits found in Planck and WiggleZ at $\ln(-\tau_0) \sim 5.3$ and $\ln(-\tau_0) \sim 5.55$, and their enhancement of 20% in likelihood improvement. The difference in the likelihood (Δ) is calculated against the best fit value of ΛCDM in the different data sets. The regions where there is no significant improvement over the best fit of the ΛCDM model are not shown.

as discussed in the previous section.

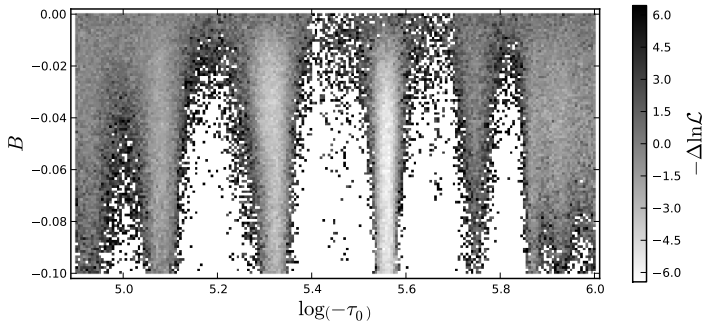

(a) MCMC sampling

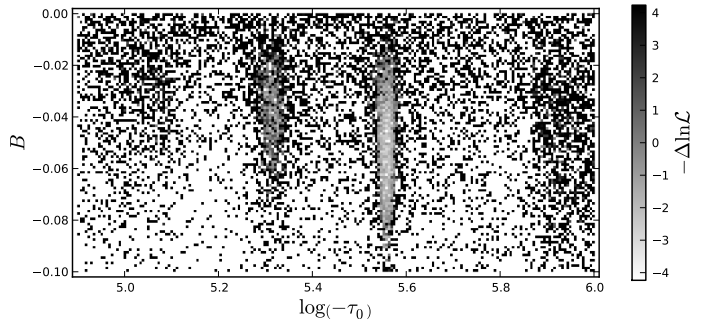

(b) Multi-modal nested sampling

Figure 3.2: Profile likelihood in the $(\ln(-\tau_0), B)$ plane for Planck+WiggleZ, for the different sampling methods. It demonstrates how the multi-modal nested sampling algorithm samples more thoroughly the regions of low likelihood. The regions not samples are shown in white (in the B&W version, not to be confused with the light grey areas of high likelihood). The difference in the likelihood (Δ) is calculated against the best fit value of ΛCDM in the different data sets.

Inspired by the fact that there exists a relatively significant reduction in the likelihood value of the feature model in the best fits compared with that of the featureless ΛCDM model, (e.g. for mode $\mathcal{B}$ the joint data analysis gives $-2\Delta \ln \mathcal{L} \sim 10$), we are motivated to compute the Bayesian ratio of the feature model. The statistical results are summarised in table 3.2, fig. 3.2(b) and fig. 3.3.

A comparison between the results of the MCMC and multi-modal nested samplings, showing the consistency between them, can be seen in fig. 3.2. The main difference between both sub-plots is due to the more thorough sampling of the tails of the distribution (points in parameter space with low likelihood value)

Model	Data set	$-2\ln\mathcal{L}$	$\ln\mathcal{Z}$	R
M_1	Planck	9801.918 (9796.27)	-4955.61 ± 0.31	$\exp(0.46) \simeq 1.6$
M_0	Planck	9807.154 (9805.90)	-4956.07 ± 0.31	
M_1	Planck+WiggleZ	10253.570 (10249.20)	-5183.05 ± 0.32	$\exp(0.62) \simeq 1.9$
M_0	Planck+WiggleZ	10262.042 (10258.80)	-5183.67 ± 0.31	

Table 3.2: Multi-modal nested sampling results of feature (M_1) and non-feature (M_0) models with the different data sets. The likelihood values in the third column are given at the best fit, first the nested sampling value, and second, in parenthesis, the MCMC sampling value.

achieved by multi-modal nested sampling: these points are crucial to get a reliable evidence estimation, which is the goal of the nested-sampling algorithms, but almost irrelevant to parameter estimation, at which MCMC excel. In table 3.2, we can see that the resulting best-fit likelihood values from multi-modal nested sampling are also consistent with those coming from MCMC sampling, though, as expected, the former a little bit lower than the latter, since the sampling around the maxima is more thorough in MCMC's.

In the first place, the Bayesian ratios listed in table 3.2 tell us that, taking into account only the part of the parameter space described in sec. 2.2, there would apparently exist a slightly positive preference for the feature model: $R \sim 1.9\,(\text{Planck} + \text{WiggleZ})$ vs. $1.6\,(\text{Planck})$ (though, according to the conventional criterion [18] it is *barely worth mentioning*). We must emphasise that in this paper we did not cover all the parameter regime allowed by theory, which sets no lower bound for τ_0, but instead the regime in which the features are most likely to be detectable by Planck. Despite the expected corrections, the slightly favourable value of the Bayesian evidence in the observable regime makes us optimistic about the enlargement of the parameter space and the addition of new data sets, namely Planck's polarisation power spectrum and bispectrum. This optimism is also backed up by how, as discussed in the sec. 3.3, the increase in the Bayesian ratio when adding the WiggleZ data indicates a positive correlation between the features found in both data sets; nevertheless, when put into the context of the error bars for the evidences cited in table 3.2, the claim gets milder.

Also, on the positive side, as can be seen in fig. 3.3, the addition of the WiggleZ data set clearly pushes the marginalised distribution towards bigger amplitudes of the feature with respect to using Planck data only, which on the one hand is an indication of a positive correlation between the sets, and on the other hand reinforces the overall likelihood of the presence of a feature against the null hypothesis.

3.5 Conclusions and outlook

In this chapter we searched for primordial oscillatory signals inspired by a transient reduction in the sound speed of the adiabatic curvature perturbation via

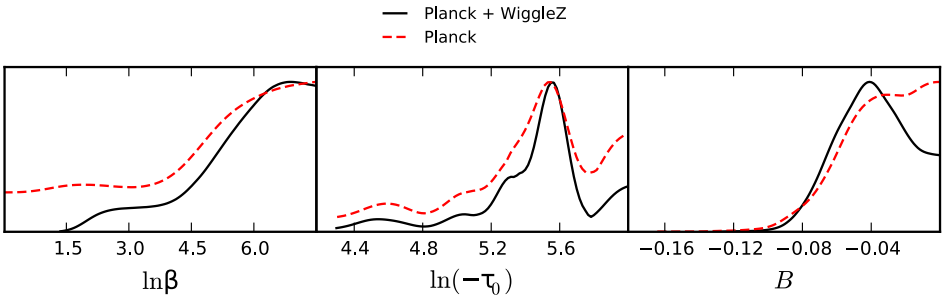

(a) 1D marginalised posterior

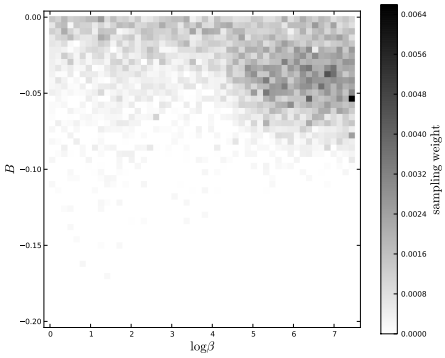

(b) Marginalised posterior for Planck

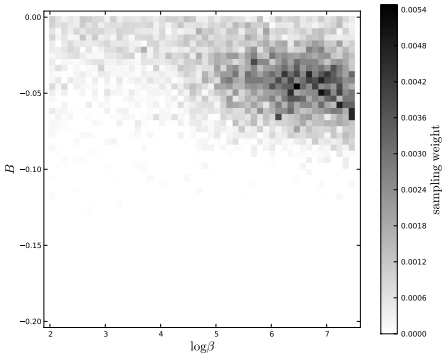

(c) Marginalised posterior for Planck+WiggleZ

Figure 3.3: Multi-modal nested sampling results: 1D marginalised posterior distribution for the feature parameters and 2D marginalised posterior distribution in the plane $(\ln \beta, B)$, with and without the WiggleZ data set. Notice how the addition of the WiggleZ data set increases the overall likelihood of a feature with a non-zero amplitude.

CMB (Planck) and LSS (WiggleZ) windows. First of all, by analysing both data sets separately, we found some common oscillatory patterns both in the Planck CMB temperature power spectrum and the WiggleZ galaxy spectrum. Interestingly, we found a coincidence in the most significant mode previously found by Achúcarro *et al.* 2013 [2] by using only Planck data. Second, the joint data analysis showed that the oscillation frequency of the feature gets better constrained, and the amplitude marginally deviates from zero, unlike what was observed by using only Planck data. Besides parameter estimation, we also calculated the Bayesian evidence for the purpose of model selection by using multi-modal nested sampling. For a full model selection study, the prior must be extended and sampled in the full parameter range allowed by the theory. Our results show that,

if we were to ignore the parts of the parameter space not sampled here, there would exist a slightly positive preference for the feature model, Bayesian factor $R \sim 1.9$ (Planck + WiggleZ), vs. 1.6 (Planck). Therefore, we are optimistic about enlarging the sampled parameter range and using additional data sets, specially Planck's polarisation power spectra and temperature bispectrum.

The Bayesian evidence analysis shows that although there exists a relatively large improvement in the likelihood value ($-2\Delta \ln \mathcal{L} \sim 10$) in several particular parameter regimes, due to the relatively large number of extra parameters (3) and their broad ranges of variation (look-elsewhere effect), the present Planck temperature and WiggleZ matter power spectra data still lack significance to claim a detection. However, due to the correlations between temperature and polarisation modes of the power spectrum and the correlations with the bispectra given by the model of transient reductions in the speed of sound, the present results have specific *predictions* for the TE cross-correlation spectrum (C_ℓ^{TE}) [1] and the temperature bispectrum ($B^{\mathrm{TTT}}_{\ell_1\ell_2\ell_3}$) [2, 1] which can be detected with the upcoming Planck data release 2014. Particularly, the new fast bispectrum estimator of oscillatory features from [23] should be able to cover the frequency where the most significant mode that we found is located.

In the light of the additional WiggleZ data, we update the predictions stated in chapter 2 and [2, 1], based on the high correlation between the bispectrum features studied there and the phenomenological oscillatory shape tested by the Planck collaboration and given in [8, eq. (16)].[5] In the parameters used by the Planck collaboration, we expect to find a feature with zero phase, and wavelength in the 95% c.l. interval $k_c \in (0.0078, 0.0083)$ from mode $\mathcal{B}$, *or* $k_c \in (0.0099, 0.0110)$ from mode $\mathcal{C}$. As happened when using only Planck data [1], a degeneracy between B and $\ln \beta$ prevents us from setting accurate predictions for the amplitude and envelope of the feature. Nevertheless, for all values of the parameters along the degeneracy, the signal is most significant on the scales beyond the second acoustic peak, and reaches its maximum around the third or fourth peak.

Bibliography

[1] Ana Achucarro, Vicente Atal, Bin Hu, Pablo Ortiz, and Jesus Torrado. Inflation with moderately sharp features in the speed of sound: GSR and in-in formalism for power spectrum and bispectrum. *Phys.Rev.*, D90:023511, 2014, 1404.7522.

[2] Ana Achucarro, Vicente Atal, Pablo Ortiz, and Jesus Torrado. Localized correlated features in the CMB power spectrum and primordial bispectrum from a transient reduction in the speed of sound. *Phys.Rev.*, D89:103006, 2014, 1311.2552.

[5] For every combination of the feature parameter values in the regions of high likelihood, one can find a combination of the parameters in [8] (including a gaussian envelope as described there) such that the correlation between both shapes at the primordial level is al least 95%.

[3] Ana Achucarro, Jinn-Ouk Gong, Sjoerd Hardeman, Gonzalo A. Palma, and Subodh P. Patil. Features of heavy physics in the CMB power spectrum. *JCAP*, 1101:030, 2011, 1010.3693.

[4] Ana Achucarro, Jinn-Ouk Gong, Sjoerd Hardeman, Gonzalo A. Palma, and Subodh P. Patil. Mass hierarchies and non-decoupling in multi-scalar field dynamics. *Phys.Rev.*, D84:043502, 2011, 1005.3848.

[5] Ana Achucarro, Jinn-Ouk Gong, Sjoerd Hardeman, Gonzalo A. Palma, and Subodh P. Patil. Effective theories of single field inflation when heavy fields matter. *JHEP*, 1205:066, 2012, 1201.6342.

[6] P.A.R. Ade et al. Planck 2013 results. XV. CMB power spectra and likelihood. 2013, 1303.5075.

[7] P.A.R. Ade et al. Planck 2013 results. XXII. Constraints on inflation. 2013, 1303.5082.

[8] P.A.R. Ade et al. Planck 2013 Results. XXIV. Constraints on primordial non-Gaussianity. 2013, 1303.5084.

[9] P.A.R. Ade et al. Planck 2013 results. XVI. Cosmological parameters. *Astron.Astrophys.*, 2014, 1303.5076.

[10] C.L. Bennett et al. Nine-Year Wilkinson Microwave Anisotropy Probe (WMAP) Observations: Final Maps and Results. *Astrophys.J.Suppl.*, 208:20, 2013, 1212.5225.

[11] C. Blake, S. Brough, M. Colless, W. Couch, S. Croom, T. Davis, M. J. Drinkwater, K. Forster, K. Glazebrook, B. Jelliffe, R. J. Jurek, I.-H. Li, B. Madore, C. Martin, K. Pimbblet, G. B. Poole, M. Pracy, R. Sharp, E. Wisnioski, D. Woods, and T. Wyder. The WiggleZ Dark Energy Survey: the selection function and z = 0.6 galaxy power spectrum. *MNRAS*, 406:803–821, August 2010, 1003.5721.

[12] Sebastian Cespedes, Vicente Atal, and Gonzalo A. Palma. On the importance of heavy fields during inflation. *JCAP*, 1205:008, 2012, 1201.4848.

[13] M. J. Drinkwater, R. J. Jurek, C. Blake, D. Woods, K. A. Pimbblet, K. Glazebrook, R. Sharp, M. B. Pracy, S. Brough, M. Colless, W. J. Couch, S. M. Croom, T. M. Davis, D. Forbes, K. Forster, D. G. Gilbank, M. Gladders, B. Jelliffe, N. Jones, I.-H. Li, B. Madore, D. C. Martin, G. B. Poole, T. Small, E. Wisnioski, T. Wyder, and H. K. C. Yee. The WiggleZ Dark Energy Survey: survey design and first data release. *MNRAS*, 401:1429–1452, January 2010, 0911.4246.

[14] F. Feroz, M. P. Hobson, E. Cameron, and A. N. Pettitt. Importance Nested Sampling and the MultiNest Algorithm. *ArXiv e-prints*, June 2013, 1306.2144.

[15] F. Feroz, M.P. Hobson, and M. Bridges. MultiNest: an efficient and robust Bayesian inference tool for cosmology and particle physics. *Mon.Not.Roy.Astron.Soc.*, 398:1601–1614, 2009, 0809.3437.

[16] Farhan Feroz and M.P. Hobson. Multimodal nested sampling: an efficient and robust alternative to MCMC methods for astronomical data analysis. *Mon.Not.Roy.Astron.Soc.*, 384:449, 2008, 0704.3704.

[17] Bin Hu and Jesús Torrado. Searching for primordial localized features with CMB and LSS spectra. 2014, 1410.4804.

[18] S.H. Jeffreys. *The Theory of Probability.* Oxford University Press, 1961.

[19] Antony Lewis and Sarah Bridle. Cosmological parameters from CMB and other data: a Monte- Carlo approach. *Phys. Rev.*, D66:103511, 2002, astro-ph/0205436.

[20] Antony Lewis, Anthony Challinor, and Anthony Lasenby. Efficient computation of CMB anisotropies in closed FRW models. *Astrophys.J.*, 538:473–476, 2000, astro-ph/9911177.

[21] Andrew R Liddle. Information criteria for astrophysical model selection. *Mon.Not.Roy.Astron.Soc.*, 377:L74–L78, 2007, astro-ph/0701113.

[22] Pia Mukherjee, David Parkinson, and Andrew R. Liddle. A nested sampling algorithm for cosmological model selection. *Astrophys.J.*, 638:L51–L54, 2006, astro-ph/0508461.

[23] M. Münchmeyer, F. Bouchet, M. Jackson, and B. Wandelt. The Komatsu Spergel Wandelt estimator for oscillations in the cosmic microwave background bispectrum. 2014, 1405.2550.

[24] D. Parkinson, S. Riemer-Sørensen, C. Blake, G. B. Poole, T. M. Davis, S. Brough, M. Colless, C. Contreras, W. Couch, S. Croom, D. Croton, M. J. Drinkwater, K. Forster, D. Gilbank, M. Gladders, K. Glazebrook, B. Jelliffe, R. J. Jurek, I.-h. Li, B. Madore, D. C. Martin, K. Pimbblet, M. Pracy, R. Sharp, E. Wisnioski, D. Woods, T. K. Wyder, and H. K. C. Yee. The WiggleZ Dark Energy Survey: Final data release and cosmological results. *Phys.Rev.*, D86(10):103518, November 2012, 1210.2130.

[25] Signe Riemer-Sørensen, David Parkinson, and Tamara M. Davis. Combining Planck with Large Scale Structure gives strong neutrino mass constraint. 2013, 1306.4153.

[26] R. Shaw, Michael Bridges, and M.P. Hobson. Clustered nested sampling: Efficient Bayesian inference for cosmology. *Mon.Not.Roy.Astron.Soc.*, 378:1365–1370, 2007, astro-ph/0701867.

[27] Skilling Sivia D. *Data Analysis; a Bayesian tutorial*. Oxford University Press, 2006.

[28] John Skilling. Nested sampling. *AIP Conference Proceedings*, 735(1):395–405, 2004.